

Hydrogen bonded frameworks containing aliphatic 3D linkers show high-capacity water vapour sorption

Phonlakrit Muang-Non,^a Carmen Zhou,^b Lauren K. Macreadie^{b*} and Nicholas G. White^{a*}

^a *Research School of Chemistry, The Australian National University, Canberra, ACT, Australia*
Email: nicholas.white@anu.edu.au, URL: www.nwhitegroup.com

^b *Department of Chemistry, University of New South Wales, Sydney, NSW, Australia*
Email: l.macreadie@unsw.edu.au, URL: https://research.unsw.edu.au/people/dr-lauren-macreadie

Size of BCP^{2H}, CUB^{2H} and TP^{2H}	2
Synthesis and characterisation	3
General remarks	3
Synthesis of Na ₂ ·BCP	4
Synthesis of TBA ₂ ·CUB	5
Synthesis of 1·BCP ₂	7
Synthesis of 1·CUB ₂	9
Crystallisation of 1·CUB₂	11
Powder X-ray diffraction (PXRD) studies	12
PXRD of 1·BCP ₂	12
PXRD of 1·CUB ₂	13
Single crystal X-ray diffraction (SCXRD) studies	15
Data collection and refinement	15
Structure of 1·BCP ₂	16
Structure of 1·CUB ₂	18
Structure of β-1·CUB ₂	19
Structure of γ-1·CUB ₂	20
Structure of δ-1·CUB ₂	21
Gas sorption studies	22
General remarks	22
N ₂ sorption experiments	22
H ₂ O sorption experiments at 293 K	23
Comparison of observed and expected H ₂ O capacities	25
References	26

Size of **BCP^{2H}**, **CUB^{2H}** and **TP^{2H}**

The Cambridge Structural Database¹ Version 5.43 + 4 updates was searched for the structures of the parent dicarboxylic acids, **BCP^{2H}**, **CUB^{2H}** and **TP^{2H}**. The dicarboxylate anions were not investigated as most of these are coordinated to metal ions and it was felt that the nature of the metal ion may affect the geometry of the group. The searches were limited to single crystal structures with no errors, 3D coordinates determined and $R_1 < 10\%$.

There are ten crystal structures of **TP^{2H}**, all of which are the unsolvated molecule (CSD codes: TEPHTH, TEPHTH12, TEPHTH14, TEPHTH15, TEPHTH16, TEPHTH17, TEPHTH18, TEPHTH19, TEPHTH20 and TEPHTH21). The distances between the carbon atoms of the carboxylic acid groups ranged from 5.731 – 5.743 Å with mean and median values of 5.738 and 5.740 Å, respectively.

There is one crystal structure of **CUB^{2H}**, which has $Z' = 2$ (FIGMAJ). The distances between the carbon atoms of the carboxylic acid groups were 5.675 and 5.681 Å (mean = 5.678 Å)

There are no crystal structures of **BCP^{2H}** in the CSD, so we searched for structures that contained substituents on the bicyclopentane part of the molecule. This returned 8 structures containing 12 unique molecules (CSD codes: AYIWEN, AYIWIR, AYIWOX, AYIZIU, LOBSIH, LOBSON, LOBZEK, UCOPEI). The distances between the carbon atoms of the carboxylic acid groups ranged from 4.854 – 4.919 Å with mean and median values of 4.88 and 4.872 Å, respectively.

While a definitive comparison between the **BCP^{2H}** structures and **TP^{2H}/CUB^{2H}** cannot be made due to the possible effects of substituents on the **BCP^{2H}** ring, it is clear that **TP^{2H}** and **CUB^{2H}** have very similar lengths while **BCP^{2H}** is significantly shorter.

Synthesis and characterisation

General remarks

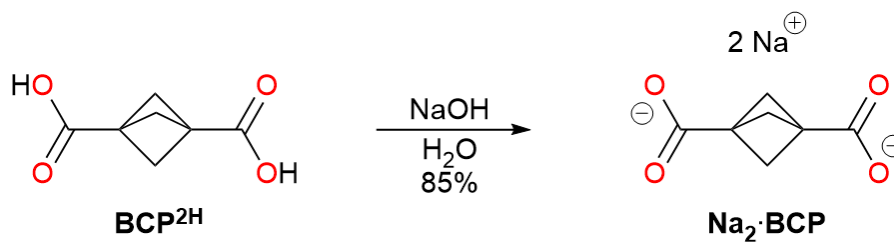
Compounds were bought from commercial suppliers with the exception of tetra-amidinium **1·Cl₄²** and bicyclopentane dicarboxylic acid **BCP^{2H,3}**, which were prepared as previously described.

NMR spectra were collected on Bruker Avance 400 or 700 spectrometers and are referenced to the residual solvent signal.⁴ Infrared spectra were recorded on a Perkin-Elmer Spectrum Two FT-IR Spectrometer (**1·CUB₂**) or Cary 630 FTIR spectrometer (**1·BCP₂**) fitted with ATR Single Reflection Diamonds. Electrospray ionisation mass spectrometry data were acquired on a Micromass Waters ZMD spectrometer. TGA data were recorded on a TA Instruments Q500 analyser (**1·CUB₂**) or TA Instruments Discovery Thermogravimetric Analyser (**1·BCP₂**) under flowing nitrogen.

Details of PXRD, SCXRD and gas sorption experiments are given in subsequent sections.

Synthesis of Na₂·BCP

The sodium salt of bicyclo[1.1.1]pentane-1,3-dicarboxylate, *i.e.* Na₂·BCP, was prepared from the dicarboxylic acid BCP^{2H,3} as shown in Scheme S1.



Scheme S1. Synthesis of Na₂·BCP.

BCP^{2H} (20 mg, 0.13 mmol) was added to a solution of NaOH (17 mg, 0.43 mmol) in H₂O (5 mL). Acetone (45 mL) was added to the solution and the mixture turned cloudy white. The mixture was centrifuged, washed with diethyl ether (3 x 15 mL) and dried under vacuum to yield white Na₂·BCP as a white powder.

Yield: 23 mg (85%).

¹H NMR (CD₃OD): 2.11 (s, 6H) ppm.

¹³C{¹H} NMR (CD₃OD): 180.3, 53.5, 40.4 ppm.

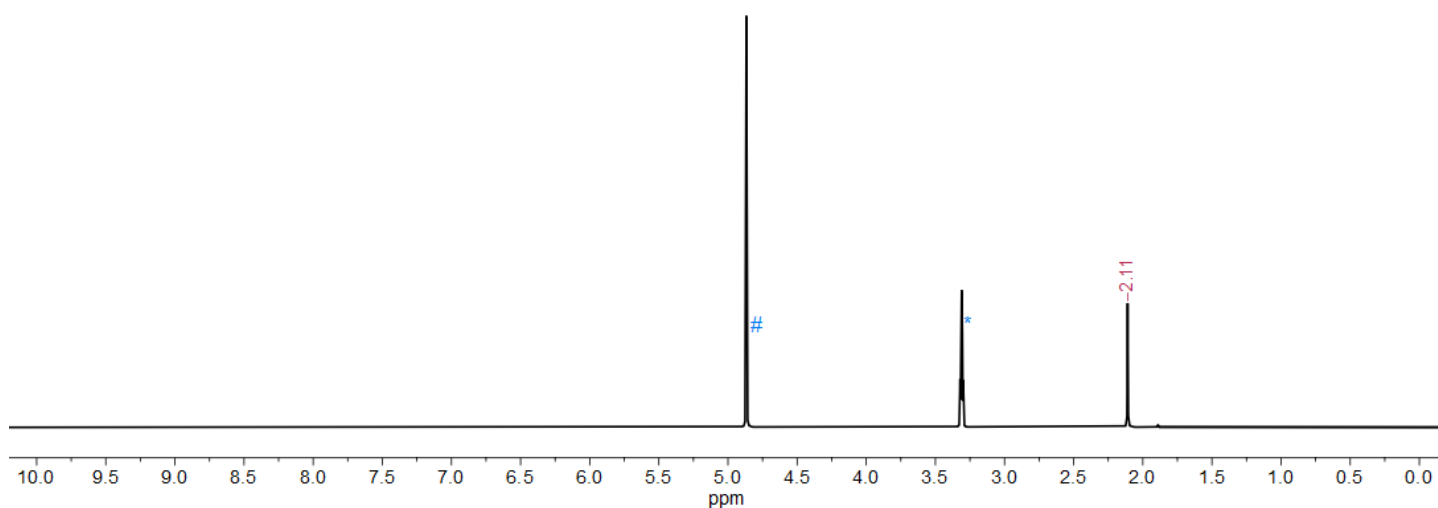


Figure S1. ¹H NMR spectrum of Na₂·BCP, peak labelled * is due to residual NMR solvent, peak labelled # is due to water (CD₃OD, 400 MHz, 298 K).

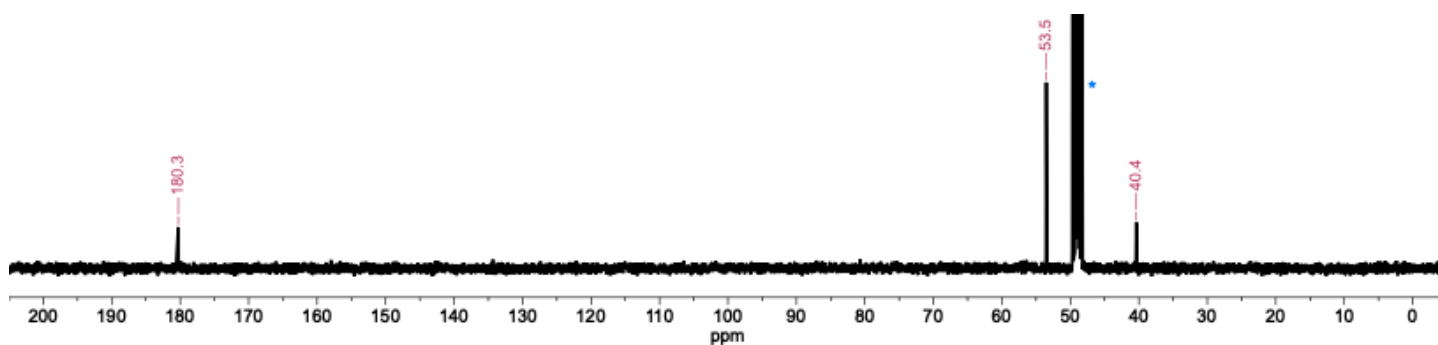
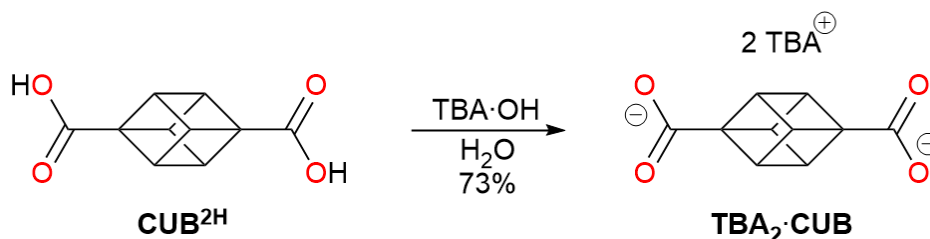


Figure S2. ¹³C{¹H} NMR spectrum of Na₂·BCP, peak labelled * is due to residual NMR solvent and has been truncated (CD₃OD, 101 MHz, 298 K).

Synthesis of TBA₂·CUB

The new tetrabutylammonium (TBA) salt of 1,4-cubanedicarboxylate, *i.e.* TBA₂·CUB, was prepared from commercially available 1,4-cubanedicarboxylic acid as shown in Scheme S2.



Scheme S2. Synthesis of TBA₂·CUB.

1,4-Cubanedicarboxylic acid (0.20 g, 1.0 mmol) was suspended in water (5 mL). Tetrabutylammonium hydroxide in methanol (1.0 M, 3.0 mL) was added to the reaction mixture and stirred for 10 minutes. The reaction mixture was dried *in vacuo*, giving a brown powder. Excess tetrabutylammonium hydroxide was removed by dissolving the crude material in hot acetone (5 mL) and precipitating using diethyl ether (20 mL). ¹H NMR spectroscopy indicated that there was excess TBA·OH present, and so the acetone/diethyl ether precipitation step was repeated twice more to remove this. The resulting white powder was isolated by filtration, washed with diethyl ether (2 × 10 mL) and air-dried.

Yield: 0.52 g (73%)

¹H NMR (D₂O): 4.06 (s, 6H), 3.21–3.23 (m, 16H), 1.65–1.70 (m, 16H), 1.36–1.41 (m, 16H), 0.97 (t, *J* = 7.4 Hz, 24H) ppm.

¹³C{¹H} NMR (D₂O): 182.3, 58.9, 58.1, 46.6, 23.1, 19.1, 12.8 ppm.

ESI-MS (neg.): 191.0340, calc. for [C₁₀H₇O₄]⁻, *i.e.* [H⁺·CUB²⁻]⁻ = 191.0349 Da.

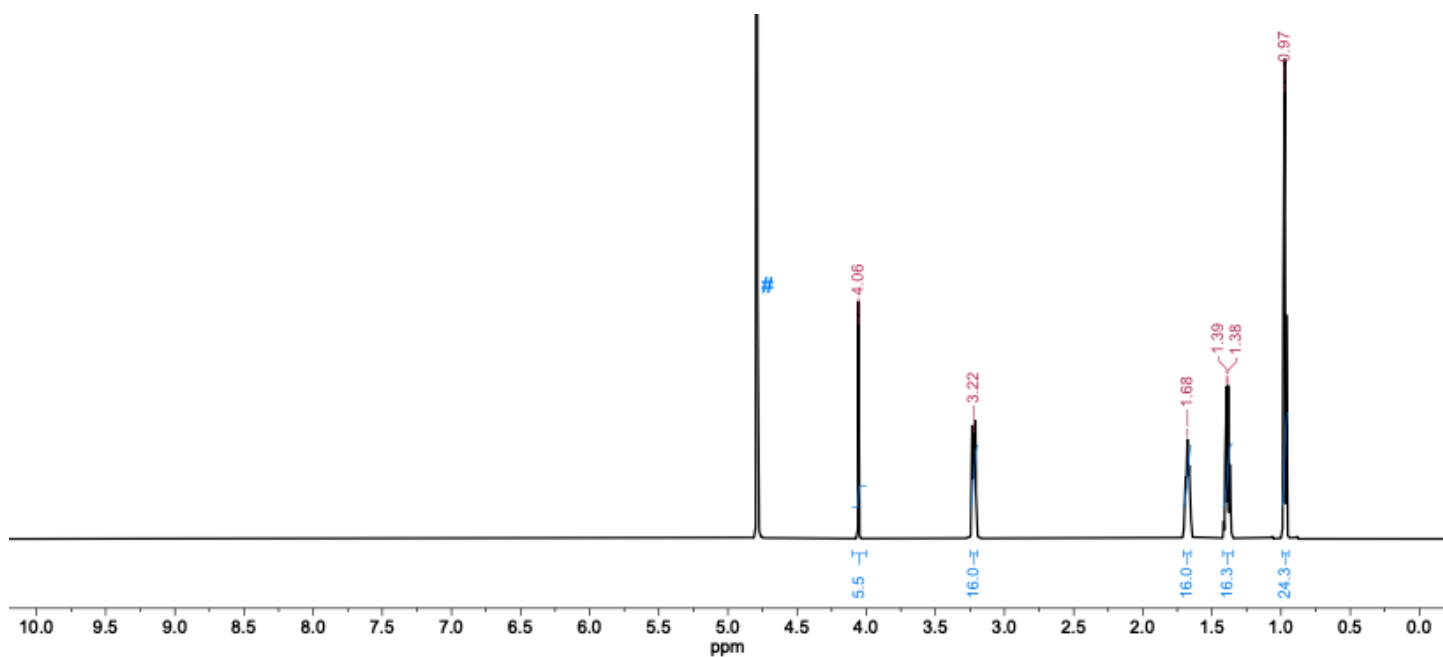


Figure S3. ^1H NMR spectrum of $\text{TBA}_2\cdot\text{CUB}$, peak labelled # is due to water (D_2O , 700 MHz, 298 K).

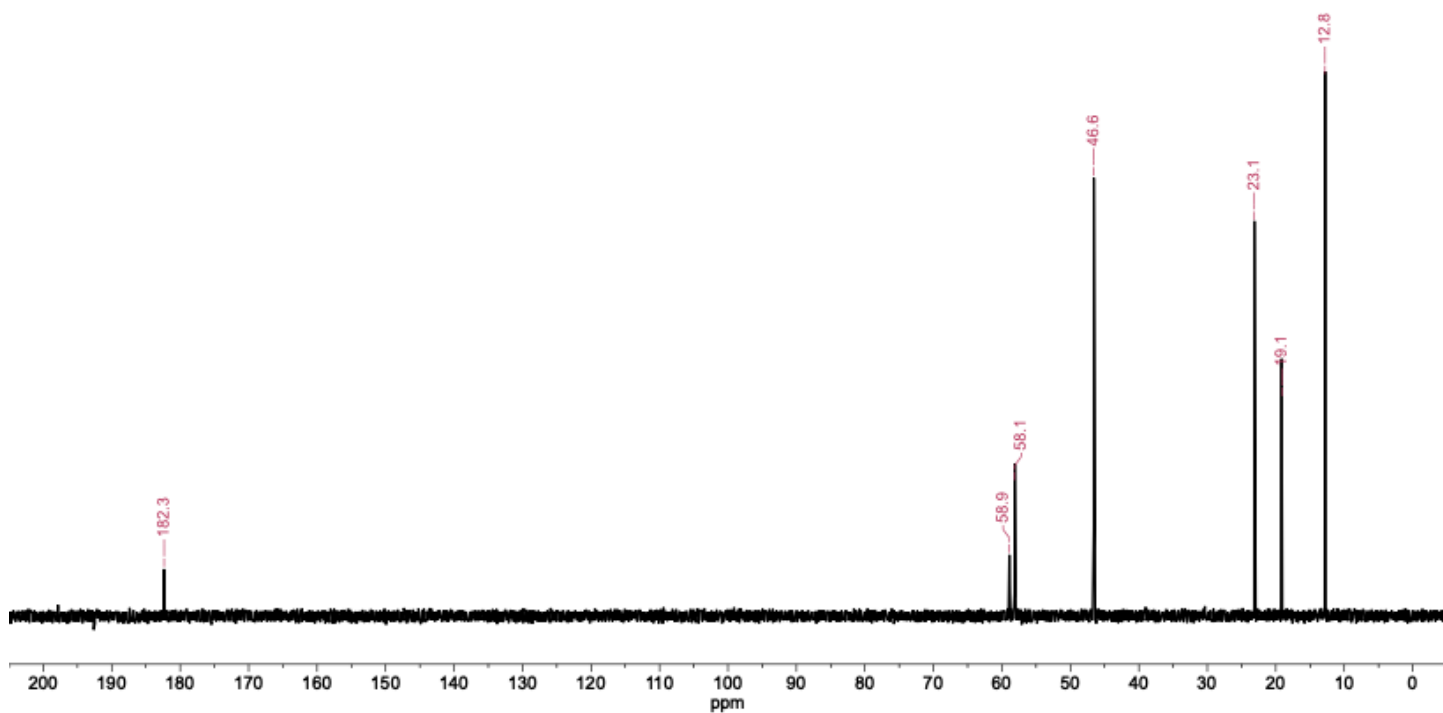


Figure S4. $^{13}\text{C}\{^1\text{H}\}$ NMR spectrum of $\text{TBA}_2\cdot\text{CUB}$ (D_2O , 176 MHz, 298 K).

Synthesis of 1·BCP₂

Na₂·BCP (15 mg, 0.097 mmol) was dissolved in 1.5:1 EtOH:H₂O (5 mL) and added to a solution of **1·Cl₄** (15 mg, 0.023 mmol) in 3:2 EtOH:H₂O (5 mL), and left to stand at room temperature. Needle crystals were observed after approximately 24 hours. After two days, the colourless, needle crystals were isolated by filtration, washed with water (3 mL) and air-dried.

Yield: 13 mg (0.042 mmol, 52%)

¹H NMR (400 MHz, d₆-DMSO containing 2 drops DCI): 7.53 (d, *J* = 8.8 Hz, 8H), 7.06 (d, *J* = 8.8 Hz, 8H), 2.08 (s, 12H) ppm. N–H peaks not observed due to H/D exchange.

ATR-IR (*inter alia*): 1684 (br., C=N stretch) 1610 (C=O stretch), 1525 (C=O stretch) cm⁻¹.

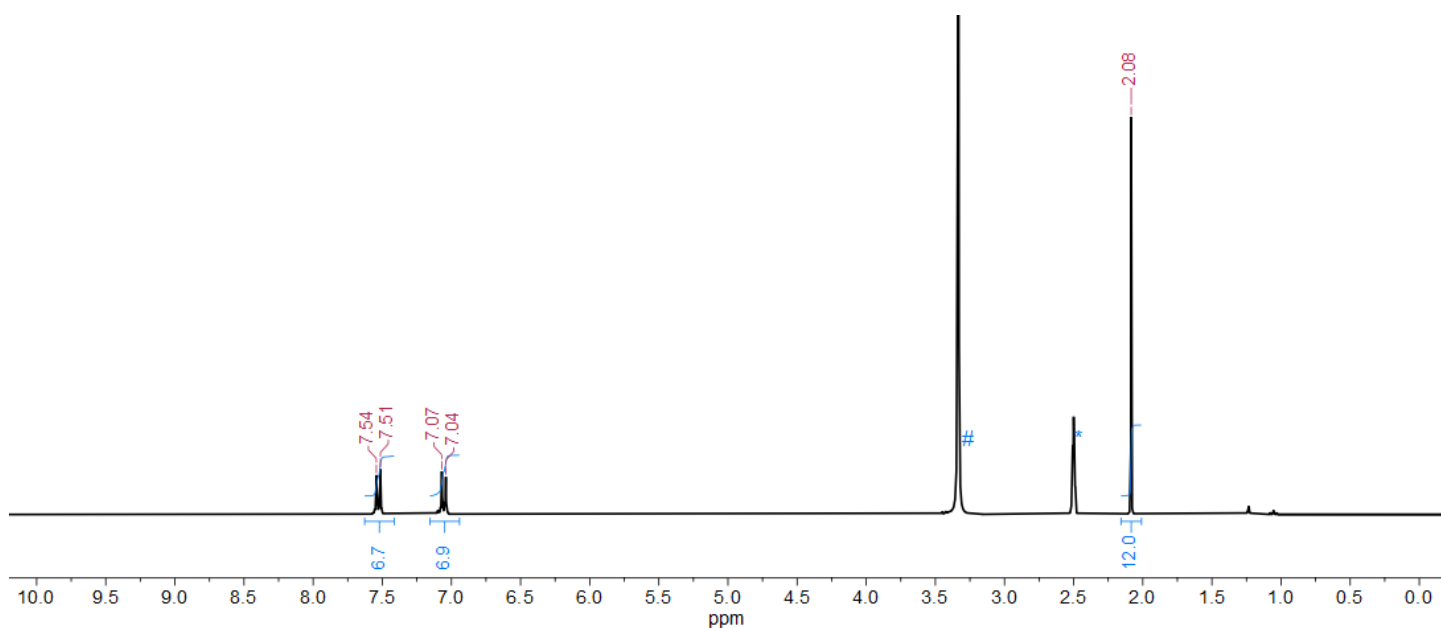


Figure S5. ¹H NMR spectrum of acid-digested **1·BCP₂**; peak labelled * results from incompletely deuterated NMR solvent, peak labelled # results from water (d₆-DMSO containing two drops DCI, 400 MHz, 298 K).

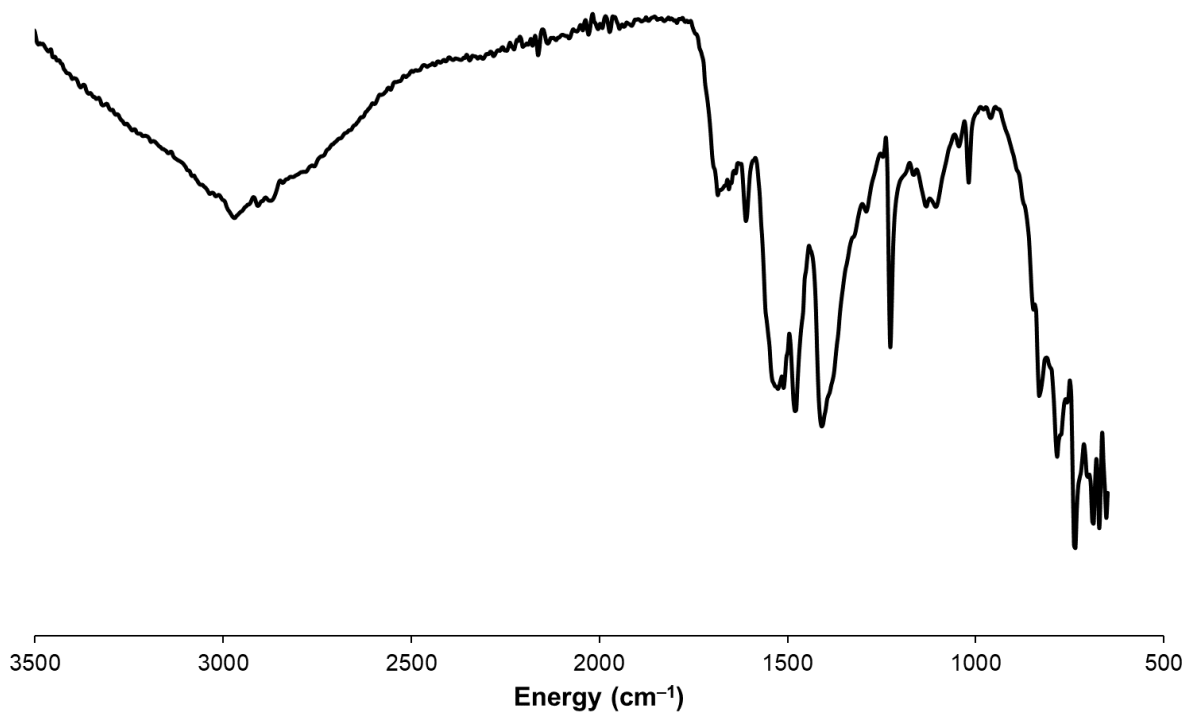


Figure S6. ATR-IR spectrum of 1·BCP₂.

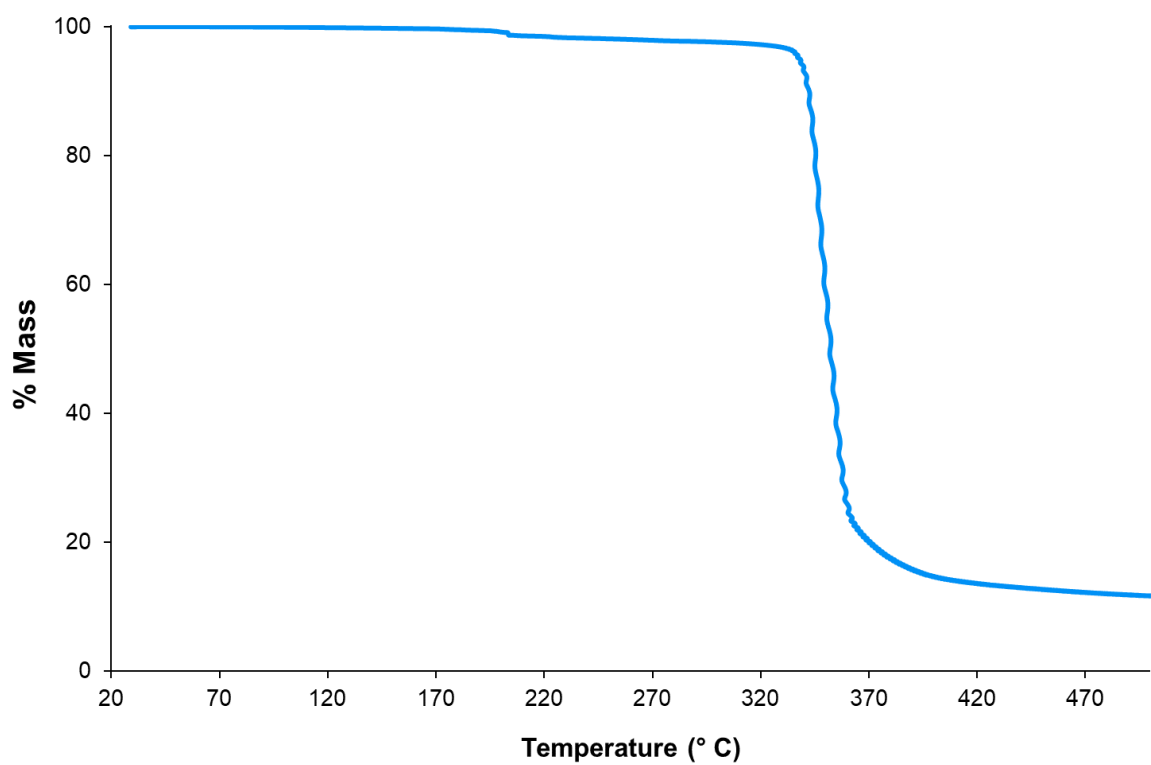


Figure S7. TGA trace of thoroughly air-dried 1·BCP₂ (recorded at a ramp rate of 10 °C/minute under N₂).

Synthesis of 1·CUB₂

These conditions give phase pure 1·CUB₂, although under different crystallisation conditions other phases can form (see Framework crystallisation summary and Table S1).

TBA₂·CUB (105 mg, 0.155 mmol) was dissolved in 4:1 EtOH:H₂O (20 mL) and added to a solution of **1·Cl₄** (49.1 mg, 0.0775 mmol) in 4:1 EtOH:H₂O (20 mL), and the resulting cloudy solution left to stand at room temperature. The cloudiness disappeared and needle crystals were observed after approximately 24 hours. After two days, the clear needle crystals were isolated by filtration, washed with water (3 mL) and air-dried.

Yield: 36.4 mg (0.0371 mmol, 48%) (assuming 6 waters per formula unit as indicated by TGA).

¹H NMR (400 MHz, d₆-DMSO containing a drop of conc. HCl_(aq)): 9.63 (br. s, 8H), 9.35 (br. s, 8H), 7.99 (d, *J* = 8.8 Hz, 8H), 7.57 (d, *J* = 8.8 Hz, 8H), 4.06 (s, 12H) ppm.

ATR-IR (*inter alia*): ~ 1650 (br, C=N stretch) 1540 (C=O stretch), 1404 (C=O stretch) cm⁻¹.

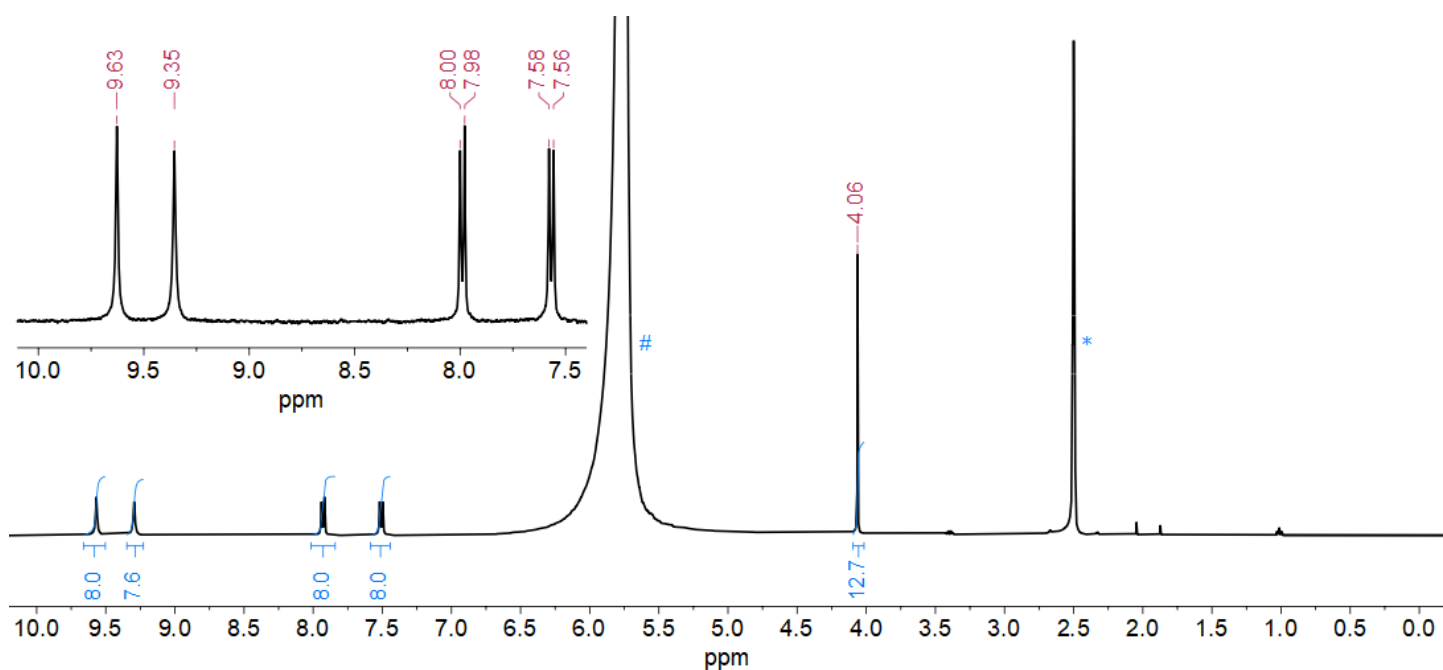


Figure S8. ¹H NMR spectrum of acid-digested 1·CUB₂; peak labelled * results from incompletely deuterated NMR solvent, peak labelled # results from water (d₆-DMSO containing 1 drop HCl_(aq), 400 MHz, 298 K).

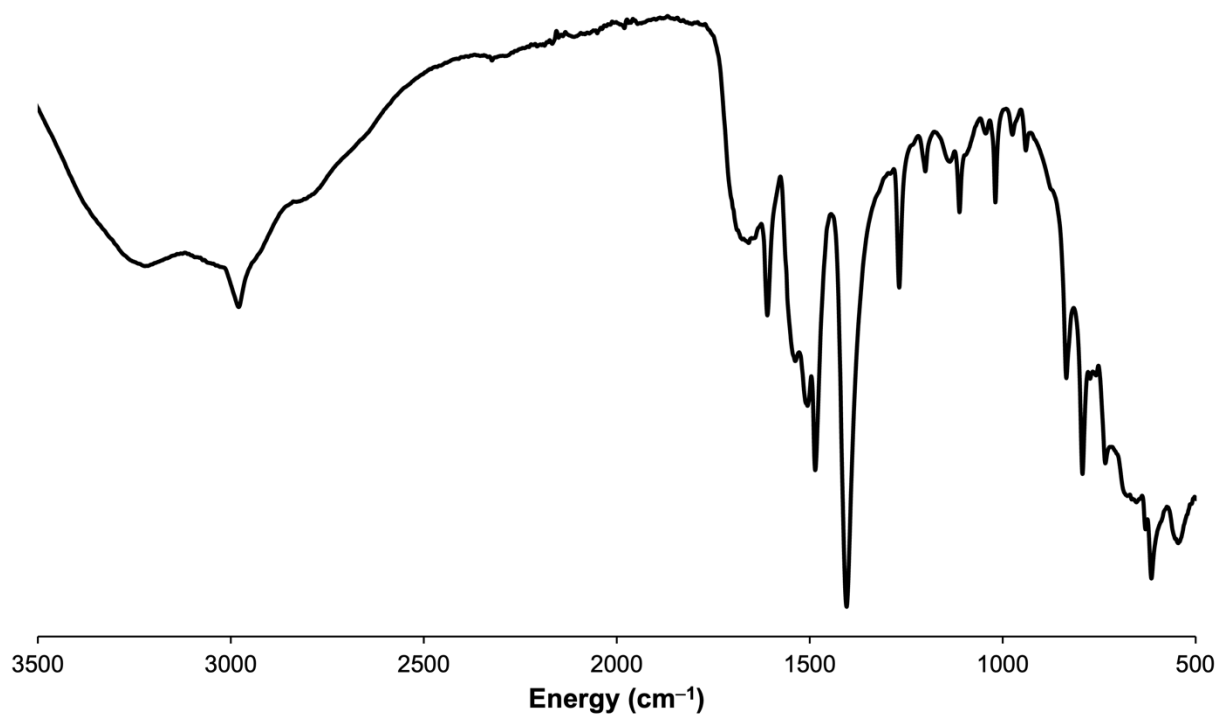


Figure S9. ATR-IR spectrum of **1-CUB₂**.

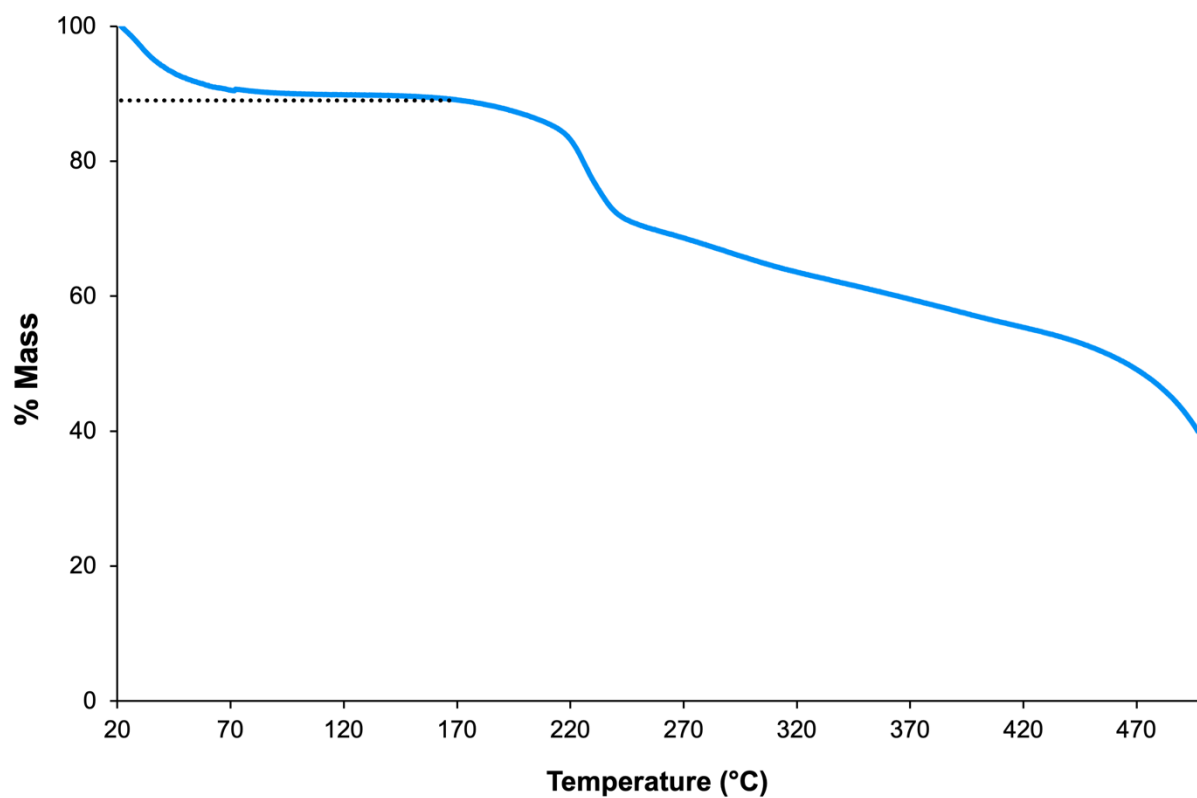


Figure S10. TGA trace of **1-CUB₂** (recorded at a ramp rate of 5 °C/minute under N₂). Dotted line shows the expected mass loss corresponding to 6 water molecules per **1-CUB₂** formula unit (89.0%).

Crystallisation of 1·CUB₂

A summary of the conditions used to crystallise 1·CUB₂ is provided in Table S1. It is notable that increasing ethanol content in the crystallisation solvent increased the speed/likelihood of crystallisation, which is in contrast to previous studies on frameworks containing aromatic dicarboxylates,⁵ including 1·TP₂.⁶

Under most tested conditions, we formed phase pure 1·CUB₂. However, growing crystals at relatively high concentrations and with low amounts of ethanol (40 or 50%) gave another phase that we term β-1·CUB₂. Heating single crystals of β-1·CUB₂ to 40 °C on a goniometer pin caused a phase change to a new phase that we term γ-1·CUB₂. If crystals were grown in solvent containing 80% ethanol at very high concentrations, or at 90% ethanol at several different concentrations, yet another phase was observed, which we term δ-1·CUB₂. The crystal structures of these phases are presented later in this document.

If crystals of 1·CUB₂ were left in the mother liquor for extended periods (~ 3 months), then they appeared to convert to β-1·CUB₂. As has previously been observed for a related amidinium···carboxylate framework,⁷ there are clearly several phases of 1·CUB₂ that have quite similar overall energies, despite having quite different hydrogen bonding arrangements. Given the similarities of the energies of these phases, it is possible that other factors such as minor variations in temperature or the glass vials used may also have effects, and this may explain the apparent lack of trend in the concentration dependence of phase in the crystallisations in 90% ethanol.

We note that while there are several other phases that can be formed, 1·CUB₂ is formed cleanly and reliably under our optimised conditions.

Table S1. Summary of crystallisation conditions and outcomes for attempted synthesis of 1·CUB₂. All crystallisations were conducted at least twice. A dash indicates no crystals formed.

% EtOH ^a	0.25 mM 1 ⁴⁺ b	0.50 mM 1 ⁴⁺ b	1.0 mM 1 ⁴⁺ b	2.0 mM 1 ⁴⁺ b	4.0 mM 1 ⁴⁺ b
0	-	-	-	-	-
10	-	-	-	-	-
20	-	-	-	-	-
30	-	-	-	-	-
40	-	-	-	-	β-1·CUB ₂
50	-	-	-	1·CUB ₂ and β-1·CUB ₂	-
60	-	-	-	1·CUB ₂	1·CUB ₂
70	-	-	1·CUB ₂	1·CUB ₂	1·CUB ₂
80	1·CUB ₂	1·CUB ₂	1·CUB ₂	1·CUB ₂	δ-1·CUB ₂
90	1·CUB ₂	δ-1·CUB ₂	δ-1·CUB ₂	1·CUB ₂ and δ-1·CUB ₂	1·CUB ₂ and δ-1·CUB ₂

^a % EtOH refers to volume % EtOH in water. ^b Concentration of CUB²⁻ was double the concentration of 1⁴⁺ in all cases.

Powder X-ray diffraction (PXRD) studies

PXRD of $1\cdot\text{BCP}_2$

PXRD patterns for $1\cdot\text{BCP}_2$ were measured at room temperature on a STOE STADI P diffractometer operating in the Debye-Scherrer geometry equipped with three Mythen detectors in stationary mode and Mo $K\alpha$ (0.7093 Å) radiation. Powder samples were wet loaded into a 0.7 mm wide glass capillary and flame sealed and rotated throughout the pattern collection. As shown in Figure S11, there is good agreement between the observed pattern and that calculated from the X-ray crystal structure.

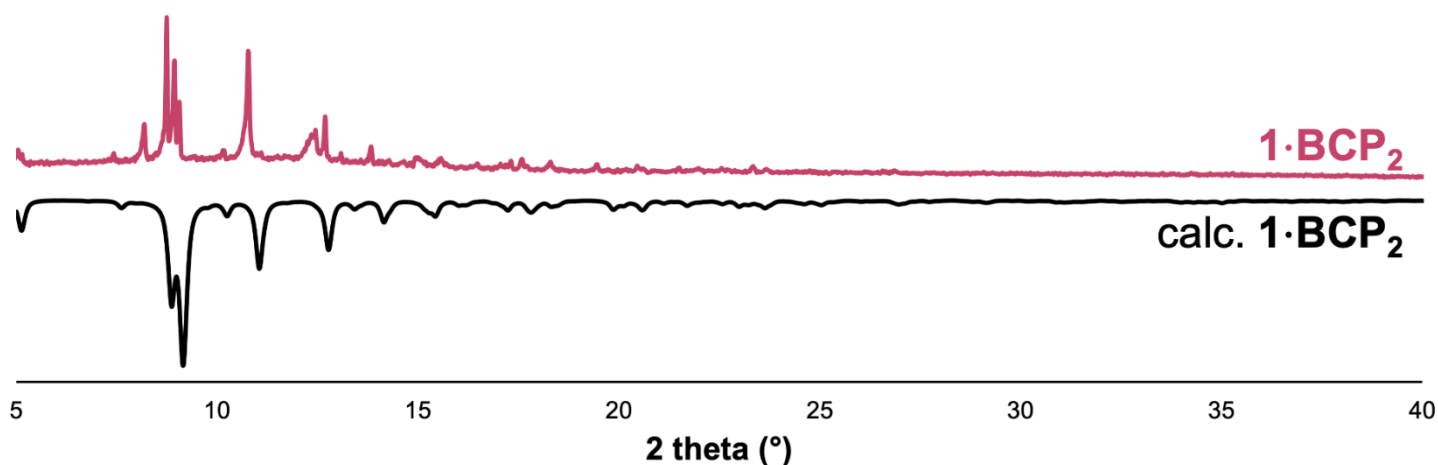


Figure S11. PXRD of $1\cdot\text{BCP}_2$ (up) and comparison with that calculated based on the single crystal structure of $1\cdot\text{BCP}_2$ (down).

PXRD of 1·CUB₂

PXRD patterns for 1·CUB₂ were recorded on a PANalytical Empyrean diffractometer using Cu K α radiation and a PIXcel detector. The PXRD patterns of 1·CUB₂ were very sensitive to sample handling. If crystals of 1·CUB₂ were isolated by decanting the solvent and transferring the crystals to a PXRD sample stage, then the observed PXRD pattern matched relatively well with that calculated from the single crystal structure, although with preferential orientation effects (Figure S12). In contrast, previously-reported 1·TP₂⁶ loses crystallinity on removal from the crystallisation solvent.

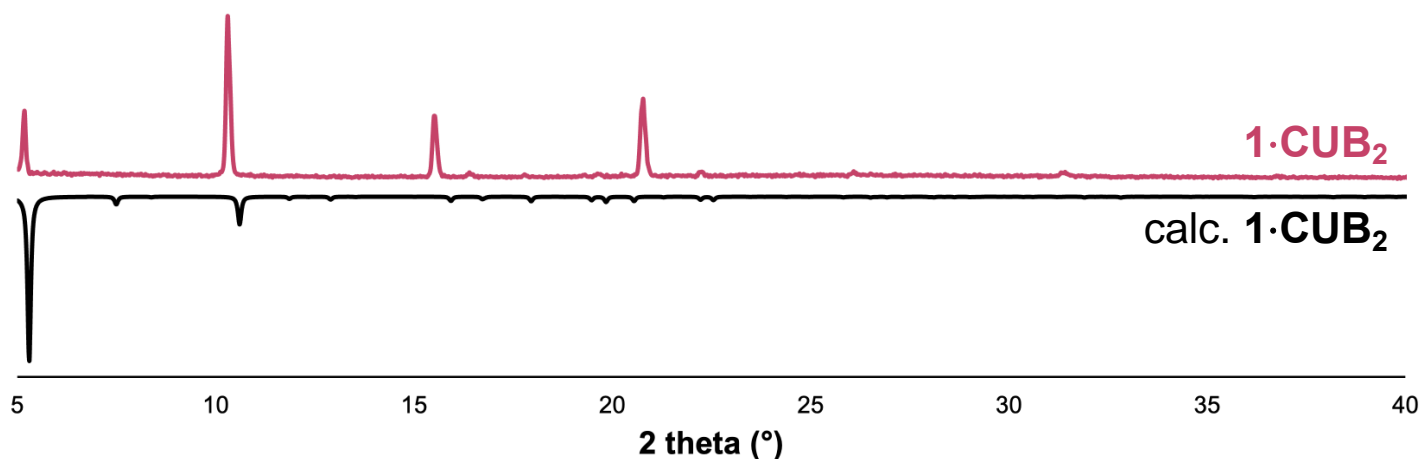


Figure S12. PXRD of 1·CUB₂ isolated by decanting solvent (up) and comparison with that calculated based on the single crystal structure of 1·CUB₂ (down).

If crystals were vacuum-dried then they transformed to a new phase that does not appear to match any of 1·CUB₂, β -1·CUB₂, γ -1·CUB₂ or δ -1·CUB₂ (Figure S13).

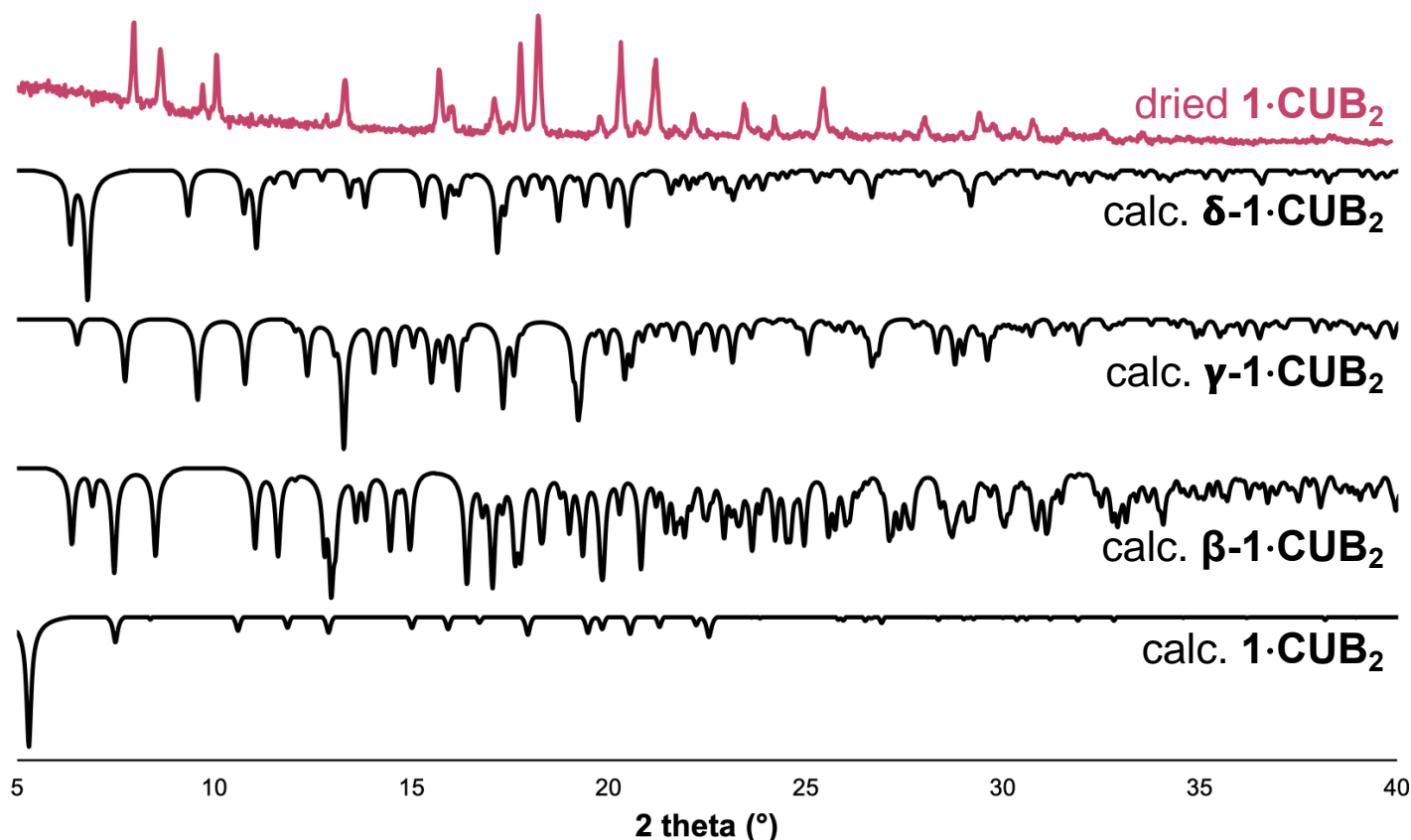


Figure S13. PXRD of vacuum-dried 1·CUB₂ (up) and comparison with those calculated based on the single crystal structure of 1·CUB₂, β -1·CUB₂, γ -1·CUB₂ and δ -1·CUB₂ (down).

If crystals of $1\cdot\text{CUB}_2$ were isolated by decanting and then studied by VT-PXRD, phase changes are observed upon heating, resulting in two new phases which first appear at 40 °C and 60 °C. These new phases do not appear to match any of $1\cdot\text{CUB}_2$, $\beta\text{-}1\cdot\text{CUB}_2$, $\gamma\text{-}1\cdot\text{CUB}_2$ or $\delta\text{-}1\cdot\text{CUB}_2$ (Figure S14). It appears that there are several accessible phases of this framework, which are broadly similar in energy, as has previously been observed for related amidinium \cdots carboxylate frameworks.⁷

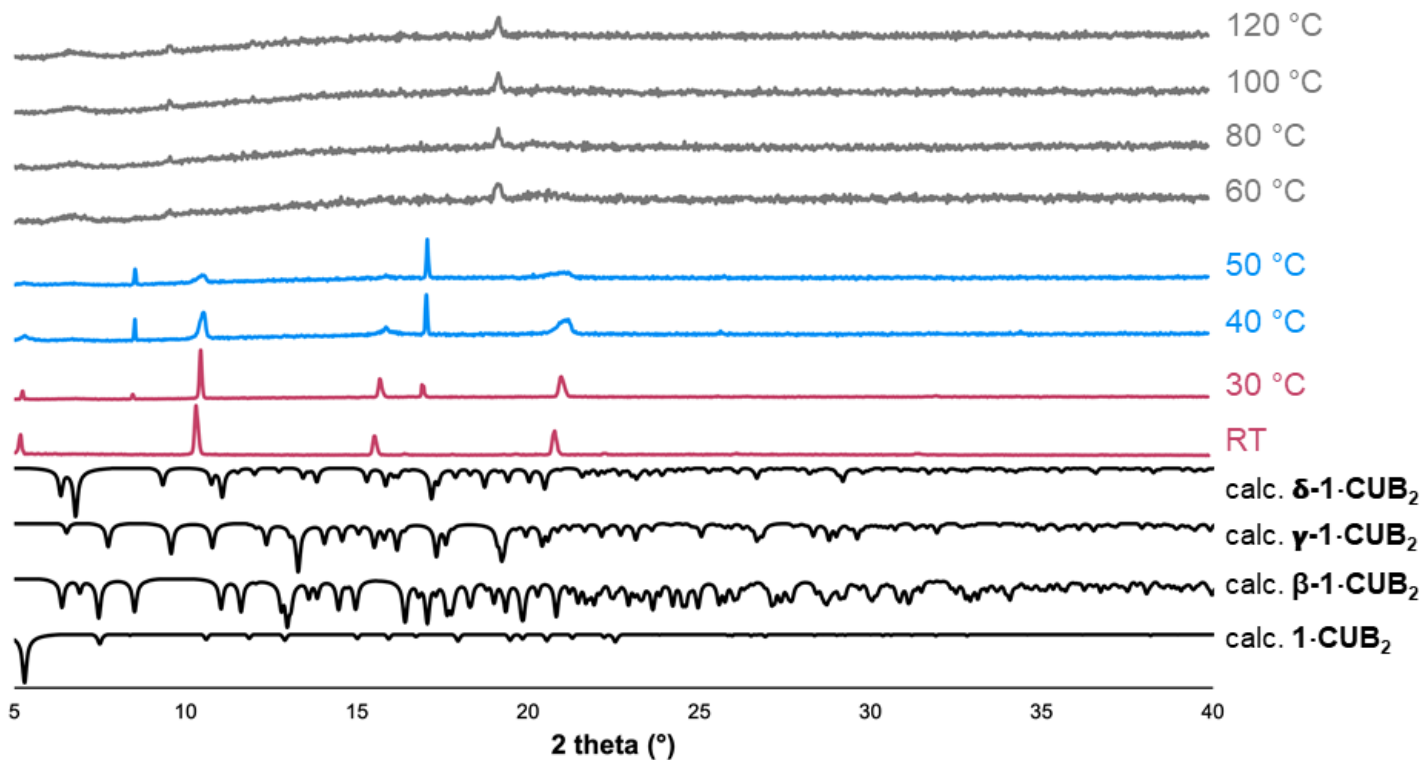


Figure S14. VT-PXRD of $1\cdot\text{CUB}_2$ isolated by decanting solvent (up) and comparison with those calculated based on the single crystal structure of $1\cdot\text{CUB}_2$, $\beta\text{-}1\cdot\text{CUB}_2$, $\gamma\text{-}1\cdot\text{CUB}_2$ and $\delta\text{-}1\cdot\text{CUB}_2$ (down).

Single crystal X-ray diffraction (SCXRD) studies

Data collection and refinement

Single crystal data for **1-CUB₂**, **β-1-CUB₂**, **γ-1-CUB₂** and **δ-1-CUB₂** were collected using mirror-monochromated Cu K α radiation on an Agilent SuperNova diffractometer. Raw frame data (including data reduction, interframe scaling, unit cell refinement and absorption corrections) were processed using CrysAlis Pro.⁸ Single crystal data for **1-BCP₂** were collected using synchrotron radiation using beamline MX2 at the Australian Synchrotron.⁹ Raw frame data for **1-BCP₂** (including data reduction, interframe scaling and unit cell refinement) were processed using XDS.¹⁰ All structures were solved using SHELXT¹¹ and refined using OLEX2.¹² All non-hydrogen atoms were refined with anisotropic displacement parameters. Hydrogen atoms were inserted using SHELX AFIX commands. For all five structures, large amounts of diffuse electron density was visible, which could not be refined. We believe this is due to poorly-ordered water molecules located in the pores of the framework. The OLEX2 solvent mask feature¹² was used to include this electron density in the refinement. Minor checkCIF alerts arise due to the unusual angles present in the bicyclopentane and cubane scaffolds.

Full crystallographic data in CIF format have been uploaded to the Cambridge Structural Database (CCDC Numbers: 2293125–2293129) and selected crystallographic data are provided in Table S2. The individual structures are discussed in the following pages, and thermal ellipsoid plots are provided in Figures S15 and S18 – S21.

Table S2. Selected crystallographic data.

Compound	1-BCP₂ ^a	1-CUB₂ ^a	β-1-CUB₂ ^a	γ-1-CUB₂ ^{a,b}	δ-1-CUB₂ ^a
Radiation type	synchrotron ($\lambda = 0.71075 \text{ \AA}$)	Cu ($\lambda = 1.54184 \text{ \AA}$)	Cu ($\lambda = 1.54184 \text{ \AA}$)	Cu ($\lambda = 1.54184 \text{ \AA}$)	Cu ($\lambda = 1.54184 \text{ \AA}$)
Temperature (K)	100	150	150	313	150
Formula	C ₂₉ H ₃₂ N ₈ · (C ₇ H ₆ O ₄) ₂ ·(H ₂ O) _{0.5} ^a	C ₂₉ H ₃₂ N ₈ · (C ₁₀ H ₆ O ₄) ₂ ^a	C ₂₉ H ₃₂ N ₈ · (C ₁₀ H ₆ O ₄) ₂ ·8H ₂ O ^a	C ₂₉ H ₃₂ N ₈ · (C ₁₀ H ₆ O ₄) ₂ ^a	C ₂₉ H ₃₂ N ₈ · (C ₁₀ H ₆ O ₄) ₂ ^a
Formula weight	809.87	872.92	1017.05	872.92	872.92
<i>a</i> (Å)	15.804(3)	23.5856(15)	13.6429(3)	13.879(5)	11.6434(3)
<i>b</i> (Å)	30.856(6)	23.5856(15)	15.3717(3)	12.595(4)	16.4405(5)
<i>c</i> (Å)	21.944(4)	7.5250(4)	16.0809(3)	27.719(12)	26.1717(8)
α (°)	90	90	62.706(2)	90	90
β (°)	101.44(3)	90	89.940(2)	102.35(4)	96.002(2)
γ (°)	90	90	63.745(2)	90	90
Unit cell volume (Å ³)	10488(4)	4186.0(6)	2600.17(11)	4733(3)	4982.4(3)
Crystal system	monoclinic	tetragonal	triclinic	monoclinic	monoclinic
Space group	P2 ₁ /n	P-4n2	P-1	I2/a	I2/a
<i>Z</i>	8	2	2	4	4
Reflections (all)	129151	5646	59597	7023	20473
Reflections (unique)	19615	2614	10469	1867	5243
<i>R</i> _{int}	0.038	0.062	0.017	0.368	0.029
<i>R</i> ₁ [<i>I</i> > 2 σ (<i>I</i>)]	0.091	0.077	0.049	0.110	0.086
<i>wR</i> ₂ (all data)	0.277	0.234	0.130	0.318	0.265
CCDC number	2293125	2293126	2293127	2293128	2293129

^a OLEX2 solvent mask used. ^b This structure was collected after heating a crystal of **β-1-CUB₂** to 313 K (resulting in a single-crystal-to-single-crystal transformation). As a result, data are of low quality.

Structure of $1 \cdot \text{BCP}_2$

Crystals were small and weakly-diffracting and it was necessary to use synchrotron radiation to obtain data with reasonable intensity. The asymmetric unit contains two molecules of 1^{4+} and four BCP^{2-} anions. One of these anions is disordered; this was modelled over two positions, with occupancies of 0.5 each. There is one well-defined water molecule located between two carboxylate groups and an amidinium group, as well as a large amount of ill-defined electron density that could not be modelled and was included in the model using the OLEX2 mask feature.¹² This removed a total of 940 e^- from a volume of 3120 \AA^3 (30% of the unit cell volume). This is consistent with the presence of ~ 94 water molecules, or approximately 12 water molecules per formula unit in addition to the one well-ordered water molecule in the asymmetric unit (which contains two formula units). It was not necessary to use any crystallographic restraints during the refinement.

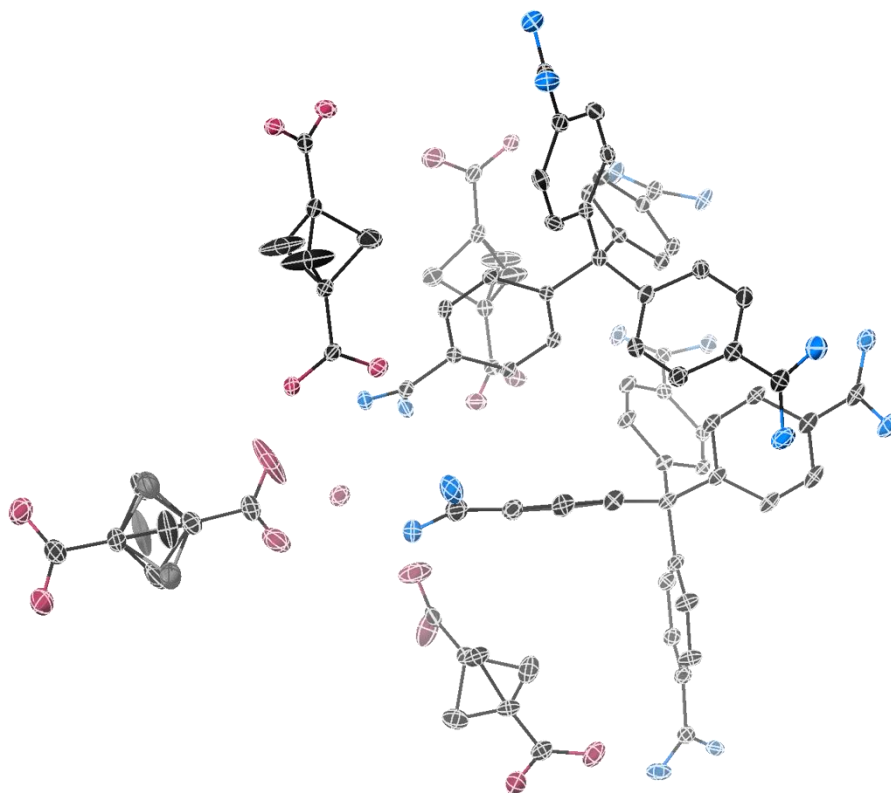


Figure S15. Thermal ellipsoid plot of the asymmetric unit of $1 \cdot \text{BCP}_2$. Thermal ellipsoids are shown at 50% probability, hydrogen atoms are omitted for clarity. OLEX2 solvent mask was used.¹² The two positions of the disordered BCP^{2-} anion are shown in different colours (black and grey).

There are a plethora of different hydrogen bonding interactions in the structure of **1·BCP₂** (Figure S16). Some of these involve a situation where both ends of a **BCP²⁻** anion bridge between the “sideways”-pointing N–H groups of two different amidinium groups on the same cation, which may be a partial explanation for why **1·BCP₂** does not form a diamondoid framework (Figure S17) while **1·CUB₂** and **1·TP₂** do. However, we note that several different phases of **1·CUB₂** were obtained, only one of which is diamondoid, and that generally predicting the structure of hydrogen bonded frameworks is extremely difficult due to the many similar energy forms that can occur.

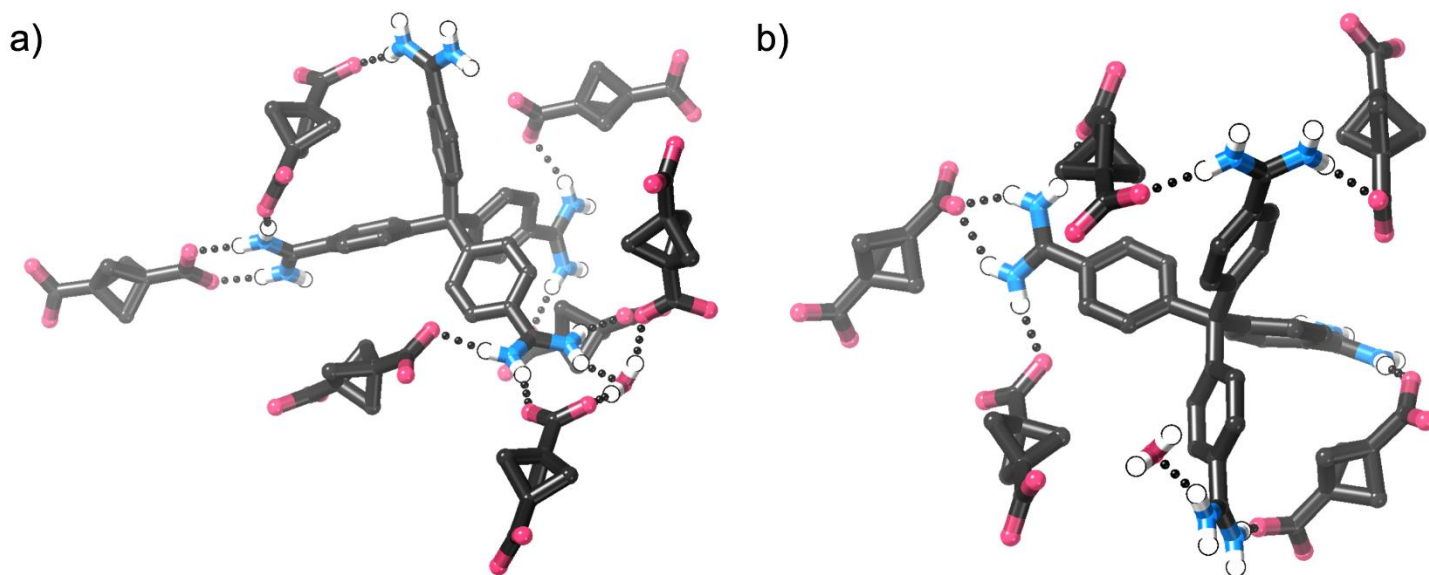


Figure S16. Diagram showing the hydrogen bonding interactions around a) the lower-numbered and b) the higher-numbered **1⁴⁺** cations in the crystal structure of **1·BCP₂** (all H···O distances less than 2.15 Å). The OLEX2 solvent mask feature was used.¹²

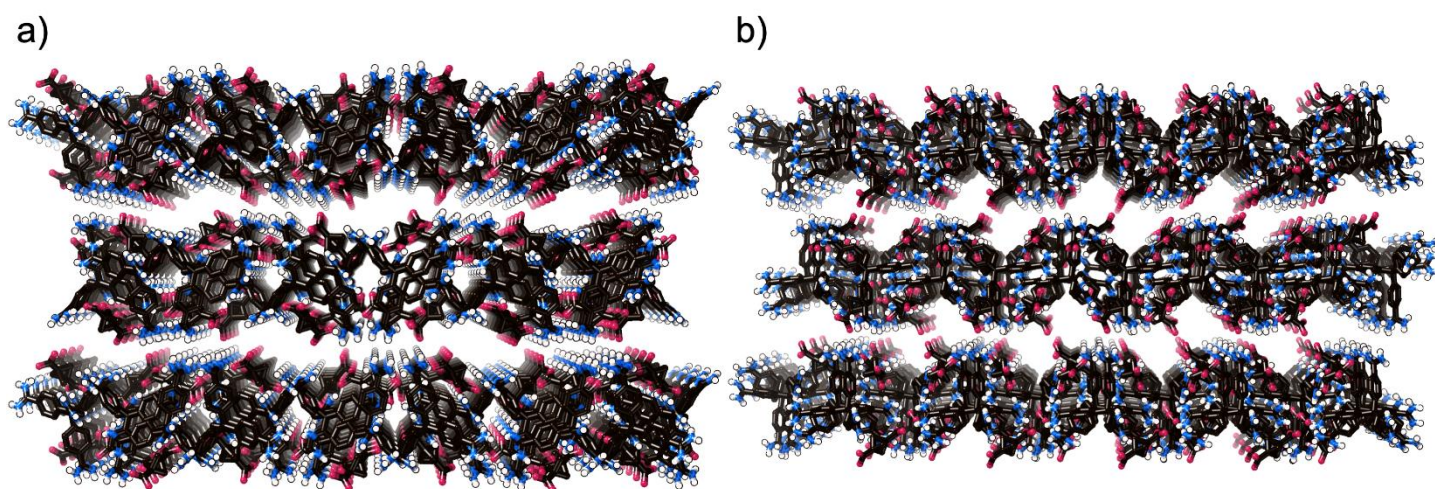


Figure S17. Diagram showing the packing of **1·BCP₂** viewed along a) the *a*-axis and b) the *c*-axis. C–H hydrogen atoms and water molecule omitted for clarity, the OLEX2 solvent mask feature was used.¹²

Structure of 1·CUB₂

Despite the use of long exposure times, it was only possible to collect diffraction data to a maximum resolution of 0.88 Å. The asymmetric unit contains one quarter of a molecule of **1**⁴⁺ and half a molecule of **CUB**²⁻. There is a large amount of diffuse electron density, believed to arise from water solvent molecules, that could not be modelled. This was included in the model using the solvent mask feature of OLEX2;¹² this removed a total of 333 e⁻ from a volume of 2302 Å³ (55% of the unit cell volume). This is consistent with the presence of ~33 water molecules, or approximately 17 water molecules per formula unit. Despite the relatively low data resolution, the structure solves and refines smoothly. It was necessary to apply DFIX restraints to the C–N bond lengths and one of the cubane C–C bond lengths (about a symmetry position), as well as RIGU restraints to the ellipsoids of the **CUB**²⁻ ellipsoid parameters in order to achieve a sensible refinement.

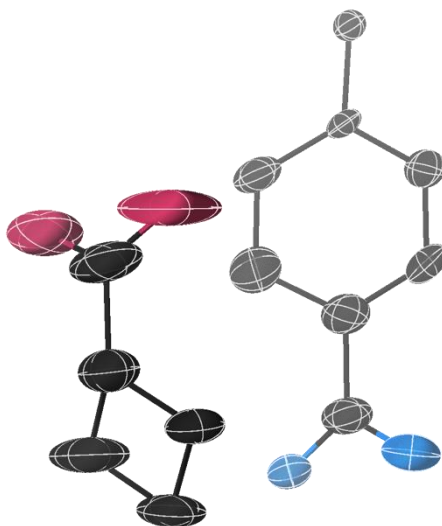


Figure S18. Thermal ellipsoid plot of the asymmetric unit of **1·CUB₂**. Thermal ellipsoids are shown at 50% probability, hydrogen atoms are omitted for clarity. OLEX2 solvent mask was used.¹²

Structure of β -1-CUB₂

The asymmetric unit contains one molecule of **1⁴⁺** as well as one full molecule and two half molecules of **CUB²⁻**. A number of water molecules could be refined sensibly, although it was necessary to add restraints to some of their hydrogen atom positions to achieve a sensible refinement. There is an additional area of diffuse electron density, believed to arise from water solvent molecules, that could not be modelled. This was included in the model using the solvent mask feature of OLEX2;¹² this removed a total of 43 e⁻ from a volume of 252 Å³ (10% of the unit cell volume). This is consistent with the presence of ~4.3 water molecules, or approximately 2 water molecules per formula unit in addition to the 8 water molecules that could be crystallographically modelled. Refinement proceeded smoothly and it was not necessary to use any crystallographic restraints during the refinement apart from those on hydrogen atom positions.

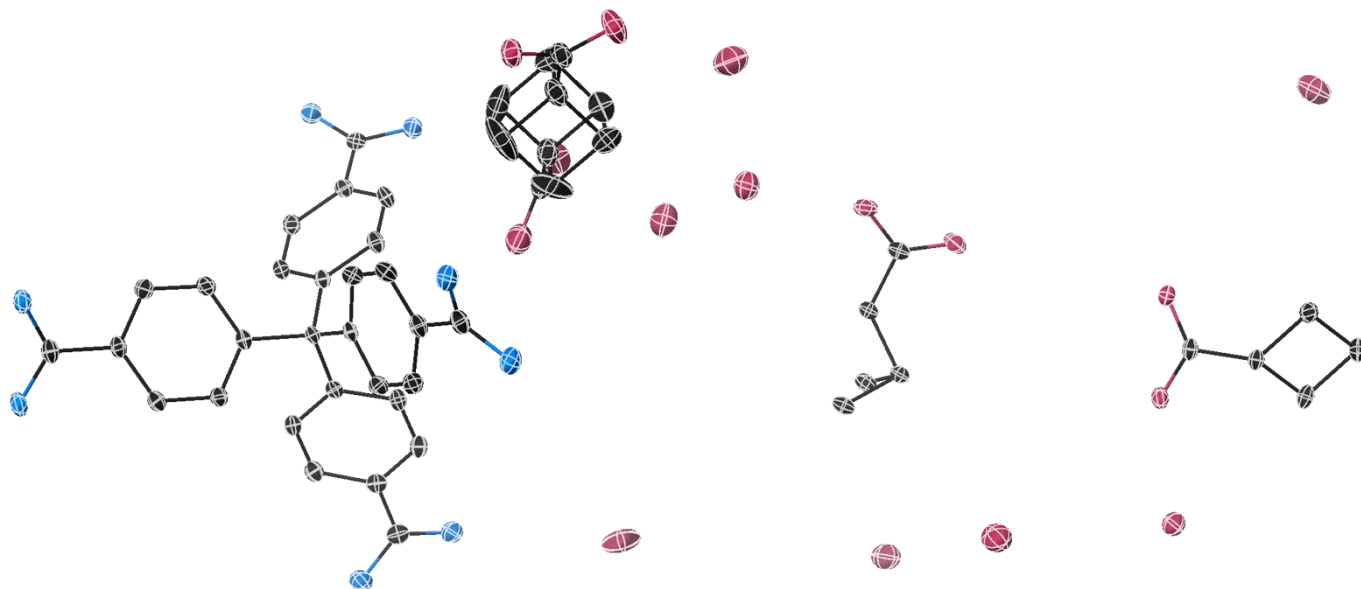


Figure S19. Thermal ellipsoid plot of the asymmetric unit of β -1-CUB₂. Thermal ellipsoids are shown at 50% probability, hydrogen atoms are omitted for clarity. OLEX2 solvent mask was used.¹²

Structure of γ -1·CUB₂

The structure of γ -1·CUB₂ was obtained by heating a single crystal of β -1·CUB₂ to 313 K on the X-ray diffractometer, and it was collected at this temperature. The crystal appeared to suffer during this process, and crystal data quality is poor. Diffraction could only be obtained to a resolution of 1.1 Å and a very high value of R_{int} was obtained (0.37). Numerous attempts were made to improve this by looking for twin laws and/or reprocessing in different space groups. However, none of these processes improved the data processing. Despite the limitations of the data, refinement proceeded smoothly and it was not necessary to use any crystallographic restraints during the refinement.

The asymmetric unit contains half a molecule of $\mathbf{1}^{4+}$ and two half molecules of \mathbf{CUB}^{2-} . There is an area of diffuse electron density, believed to arise from water solvent molecules, that could not be modelled. This was included in the model using the solvent mask feature of OLEX2;¹² this removed a total of 96 e⁻ from a volume of 886 Å³ (19% of the unit cell volume). This is consistent with the presence of ~9.6 water molecules, or approximately 2.4 water molecules per formula unit.



Figure S20. Thermal ellipsoid plot of the asymmetric unit of γ -1·CUB₂. Thermal ellipsoids are shown at 50% probability, hydrogen atoms are omitted for clarity. OLEX2 solvent mask was used.¹²

Structure of δ -1·CUB₂

The asymmetric unit contains half a molecule of **1**⁴⁺ as well as two half molecules of **CUB**²⁻. One of the phenyl rings of **1**⁴⁺ is disordered. This was modelled over two positions (occupancies 0.5 each) and it was necessary to restrain the C–C bond lengths of this disordered group using DFIX restraints in order to achieve a sensible refinement. There is an area of diffuse electron density, believed to arise from water solvent molecules, that could not be modelled. This was included in the model using the solvent mask feature of OLEX2;¹² this removed a total of 266 e⁻ from a volume of 996 Å³ (20% of the unit cell volume). This is consistent with the presence of ~27 water molecules, or approximately 6.7 water molecules per formula unit.

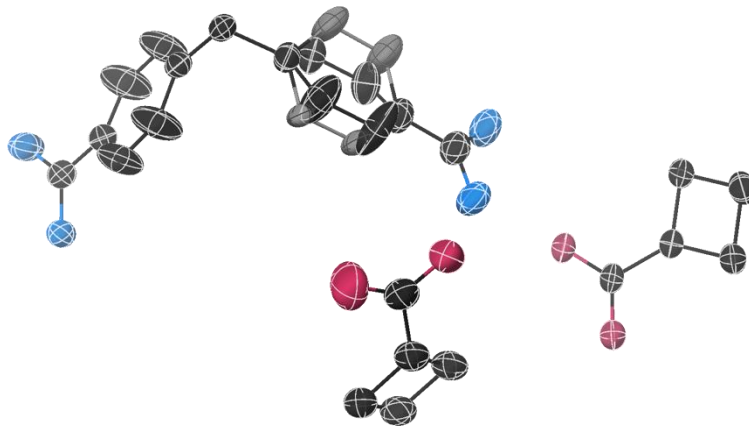


Figure S21. Thermal ellipsoid plot of the asymmetric unit of δ -1·CUB₂. Thermal ellipsoids are shown at 50% probability, hydrogen atoms are omitted for clarity. OLEX2 solvent mask was used.¹² The two positions of the disordered phenyl ring are shown in different colours (black and grey).

Gas sorption studies

General remarks

Approximately 40 mg of dried sample was weighed in a pre-dried and weighed Quartz BET tube. Adsorption isotherms for pressures in the range of 0 – 1.2 bar were measured by a volumetric method using a Micromimetics 3Flex. Measurements were performed using ultra-high purity (99.99%) N₂ gas and degassed distilled water. Samples were evacuated and activated at 100 °C under dynamic vacuum at 10⁻⁶ Torr for 24 hrs to remove residual solvent molecules.

N₂ sorption experiments

None of the frameworks show appreciable N₂ sorption (Figure S22).

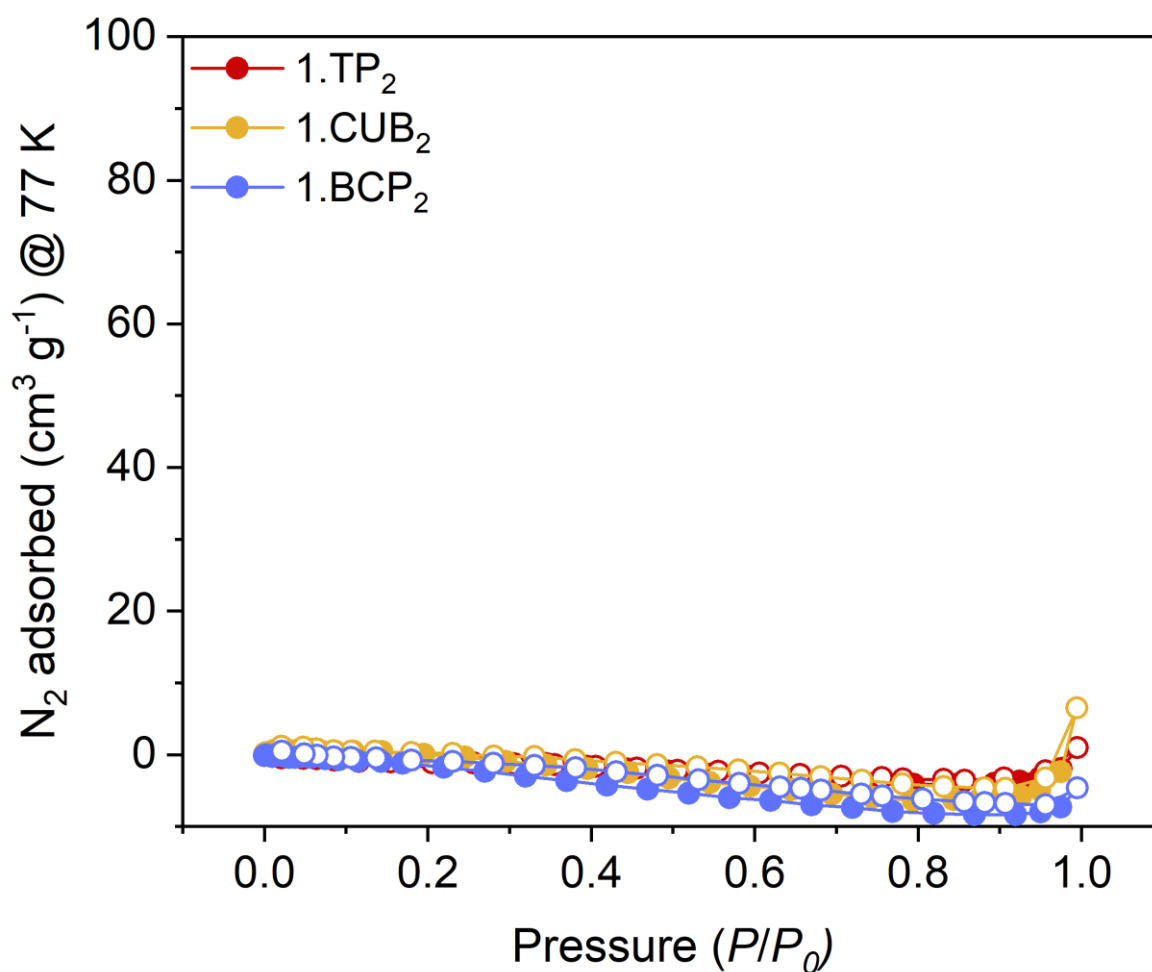


Figure S22. N₂ sorption isotherms for 1·BCP₂, 1·CUB₂ and 1·TP₂ at 77 K. Lines joining data points are intended to aid visualisation and do not represent fitting of the data.

H₂O sorption experiments at 293 K

H₂O sorption data recorded at 273 K are presented in the main text of the paper. Initially, water adsorption isotherms were recorded with 5 collection pressure points between 0 and 100 % relative humidity (RH) to find the optimum pressure steps to run the experiment. The samples were then degassed again by heating under vacuum and the next measurement was taken with several more collection pressure points at designated areas where likely step changes may be observed. If step changes were missed the samples were again degassed and additional collection pressure points were entered into the experimental method on the instrument to ensure that a complete isotherm was collected. We note that several isotherms were collected on each sample (at a minimum: the initial 5 points, then the 273 K isotherm then the 293 K isotherm), and no change was observable in the isotherms at a given temperature, indicating that water vapour sorption is reversible.

The isotherms at 273 K are shown in Figure S23 and compared with data recorded at room temperature (293 K). The overall water sorption is relatively similar at 273 and 293 K, but the steps in the sorption isotherms for **1·BCP₂** and **1·CUB₂** move to higher partial pressure at higher temperature. In the case of **1·CUB₂**, the step also becomes less pronounced.

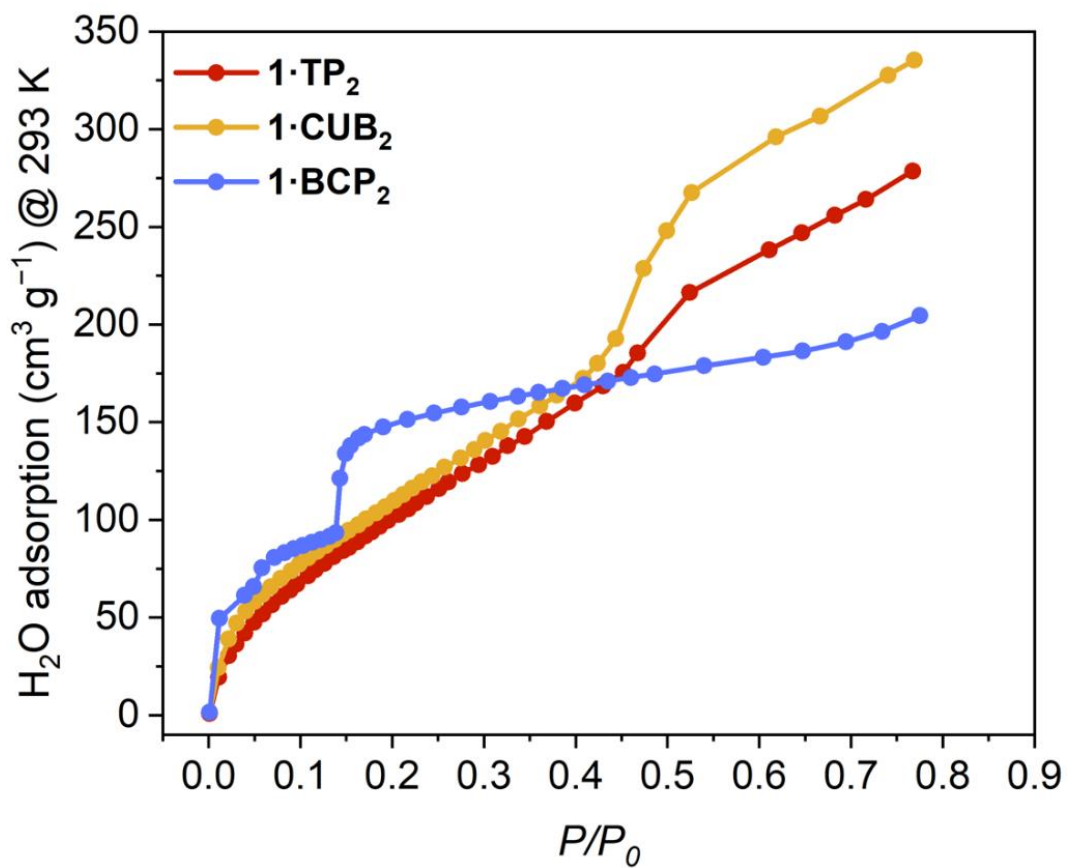
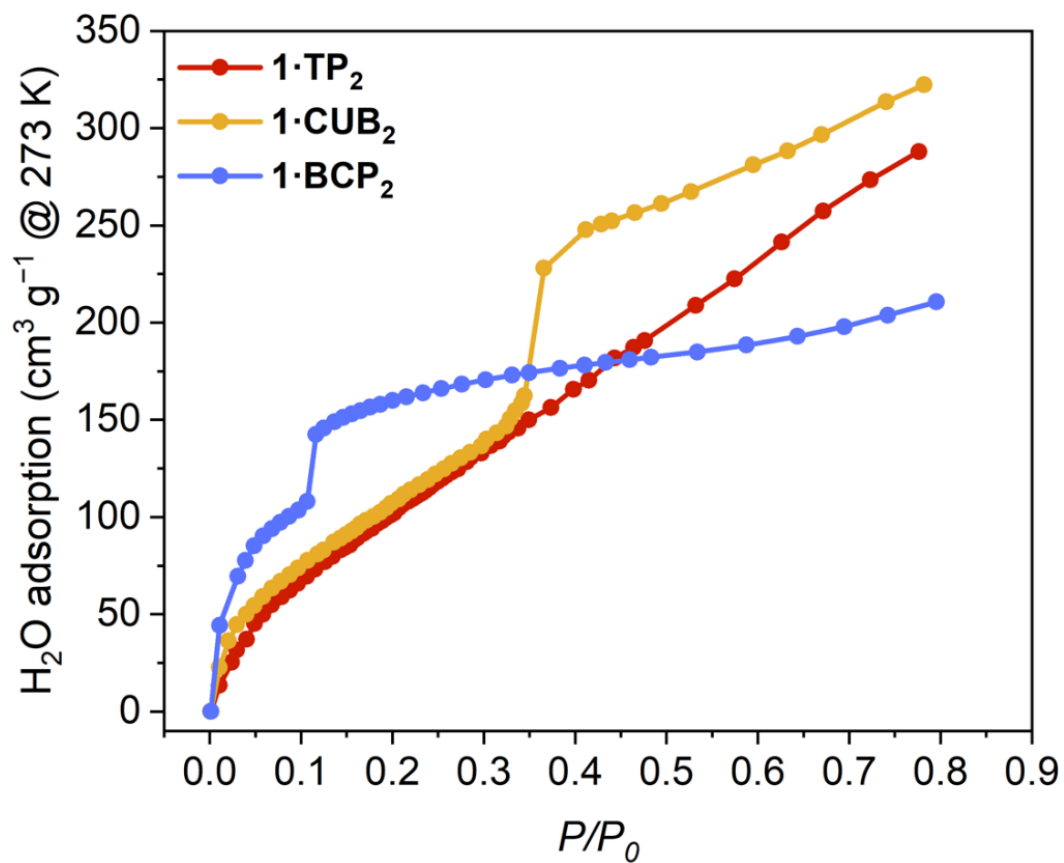


Figure S23. Water vapour sorption isotherms for **1·BCP₂**, **1·CUB₂** and **1·TP₂** at 273 K and 293 K. Lines joining data points are intended to aid visualisation and do not represent fitting of the data.

Comparison of observed and expected H₂O capacities

The water sorption data displayed in Figure S23 were compared with that expected based on the single crystal structures. We do not think that the water content of a crystal freshly removed from solvent should necessarily match perfectly that determined using vapour sorption measurements on bulk material, but in fact surprisingly good concordance is observed. **We highlight that we make several assumptions in this comparison, which should be considered as an approximation only.**

Crystals were freshly removed from solvent. This solvent was a mixture of ethanol and water, but we assume that the solvent in the pores of the material is only water, which is consistent with previous related frameworks where this solvent has been identified crystallographically.² Given the crystals were freshly removed from solvent, we felt that it was sensible to extrapolate the water sorption data to $P/P_0 = 1$. This was done by taking the water sorption data at 293 K, fitting a linear trendline to the final part of the isotherm (all datapoints at $P/P_0 > 0.5$) and using this trendline to extrapolate to $P/P_0 = 1$. This gave extrapolated expected sorption values of 400, 327 and 225 cm³ g⁻¹ for **1·CUB₂**, **1·TP₂** and **1·BCP₂** respectively.

The water content in the framework was estimated from the crystal structures. In the previously-reported structure of **1·TP₂**, the water molecules could be resolved so the actual water content was used. In the case of **1·CUB₂**, the water molecules could not be resolved and so the solvent electron density was accounted for using the OLEX2 mask feature.¹² In the case of **1·BCP₂**, there is one very tightly bound and well-resolved water molecule in the structure, while the rest are poorly-resolved and had to be included in the model using the OLEX2 mask feature. If the well-resolved water molecule was deleted, it was too close to the rest of the molecule for OLEX2 to account for it without changing the default settings, which would make comparison with other structures difficult. Therefore the OLEX2 mask feature was used to estimate the solvent content of the pore and then this water molecule was added to the number. The estimated water content for each structure based on this analysis is given in Table S3. We note that the number of water molecules observed in the crystal structures is different from that observed by TGA, but we suggest that this is not surprising given that crystals freshly removed from solvent are in a far more humid environment than the air-dried crystals used for TGA.

Table S3. Comparison of estimated expected and observed water sorption parameters.

Structure	Void volume in A ³ (unit cell) ^a	Electrons in void (unit cell) ^a	Formula units per unit cell	Water molecules per formula unit ^b	Expected water uptake (mmol g ⁻¹)	Expected water uptake (cm ³ g ⁻¹)	Water sorption at $P/P_0 = 1$ ^c (cm ³ g ⁻¹)
1·BCP₂	3119	941	8	12.3	15.3	275	225
1·CUB₂	2301	333	2	16.7	19.1	344	400
1·TP₂	–	–	4	18.8	22.9	413	327

^a Determined using OLEX2 mask feature using a probe radius of 1.2 Å. ^b Calculated based on electron count in void and/or identified crystallographically, with each water having 10 electrons. ^c Extrapolated from experimental vapour sorption measurements, as described above.

References

- 1 R. Taylor and P. A. Wood, *Chem. Rev.*, 2019, **119**, 9427–9477.
- 2 S. A. Boer, L. Conte, A. Tarzia, M. T. Huxley, M. G. Gardiner, D. R. T. Appadoo, C. Ennis, C. J. Doonan, C. Richardson and N. G. White, *Chem. Eur. J.*, 2022, **28**, e202201929.
- 3 P. Kaszynski and J. Michl, *J. Org. Chem.*, 1988, **53**, 4593–4594.
- 4 H. E. Gottlieb, V. Kotlyar and A. Nudelman, *J. Org. Chem.*, 1997, **62**, 7512–7515.
- 5 P. Muang-Non, H. D. Toop, C. J. Doonan and N. G. White, *Chem. Commun.*, 2022, **58**, 306–309.
- 6 M. Morshedi, M. Thomas, A. Tarzia, C. J. Doonan and N. G. White, *Chem Sci*, 2017, **8**, 3019–3025.
- 7 S. A. Boer, L.-J. Yu, T. L. Genet, K. Low, D. A. Cullen, M. G. Gardiner, M. L. Coote and N. G. White, *Chem. Eur. J.*, 2021, **27**, 1768–1776.
- 8 *CrysAlis Pro*, Oxford Diffraction, 2011.
- 9 D. Aragao, J. Aishima, H. Cherukuvada, R. Clarken, M. Clift, N. P. Cowieson, D. J. Ericsson, C. L. Gee, S. Macedo, N. Mudie, S. Panjikar, J. R. Price, A. Riboldi-Tunnicliffe, R. Rostan, R. Williamson and T. T. Caradoc-Davies, *J. Synchrotron Radiat.*, 2018, **25**, 885–891.
- 10 W. Kabsch, *Acta Crystallogr. D, Biol. Crystallogr.*, 2010, **66**, 125–132.
- 11 G. Sheldrick, *Acta Crystallogr. A*, 2015, **71**, 3–8.
- 12 O. V. Dolomanov, L. J. Bourhis, R. J. Gildea, J. A. K. Howard and H. Puschmann, *J. Appl. Crystallogr.*, 2009, **42**, 339–341.